

Development and validation of a real time flow control integrated MPPT charger for solar PV applications of vanadium redox flow battery

Ankur Bhattacharjee*, Hiranmay Samanta, Nipak Banerjee, Hiranmay Saha

Centre of Excellence for Green Energy and Sensor Systems, IEST, Shibpur, India



ARTICLE INFO

Keywords:

Solar PV
Vanadium Redox Flow Battery (VRFB)
Charge controller
Optimal flow rate
Efficiency

ABSTRACT

In this paper a real time flow control integrated solar PV Maximum Power Point Tracking (MPPT) charge controller for Vanadium Redox Flow battery (VRFB) is developed and its performance is demonstrated under practical dynamic insulation profiles. Unlike the conventional Lead acid and Li-ion batteries the major challenge in designing the solar MPPT charger for VRFB lies in simultaneous control of charging current and corresponding flow rate for maintaining the maximum overall system efficiency of the VRFB besides achieving the maximum charging efficiency. In this work, the usual Perturb & Observe (P&O) algorithm for designing MPPT charger for conventional batteries has been significantly modified in case of VRFB charge controller by including the real time control of flow rate along with the charging current. The proposed charging algorithm has been validated by a practical 1 kW 6 h VRFB system operation. The modified MPPT based three stage constant current constant voltage (CC-CV) charging topology is found to be the most efficient for VRFB charging from solar PV. Solar MPPT charging of VRFB with a constant flow rate leads to premature thermal shut down of the charge controller resulting incomplete charging of VRFB which is prevented by the use of dynamic flow control integrated solar PV MPPT charging. Two practical case studies of sunny weather and cloudy weather conditions have been adopted for validation of the integrated MPPT charge controller. The proposed VRFB charging system is a generalised one and thus can be very useful for large scale VRFB application in solar PV power systems.

1. Introduction

Battery energy storage systems (BESS) are drawing great interest in the field of renewable energy applications such as solar PV, wind etc. For large-scale renewable power systems, Vanadium Redox Flow Battery (VRFB) is being considered as one of the most potential BESS because of its several merits; such as, independent scalability of its power and energy capacity, deep discharge capacity, free from cross-contamination and above all its very long life cycle, closely matching to that of a solar PV power plant [1]. The VRFB technology was developed by Maria Skylas-Kazacos [2] and her research group at University of New South Wales (UNSW) in the mid-1980s. Over the years, efforts to make the VRFB technology [3–5] more efficient has led to several avenues of research like stack design [6], modifications to the electrode [7,8], membrane [9,10] and electrolyte [11–13] materials. The realisation of practical VRFB operation and performance remains incomplete without an electrical equivalent model [14–17]. A recent work published by Bhattacharjee et al. [18] proposed a generalised electrical equivalent model of VRFB system where the dynamic optimal flow rate was estimated to improve the VRFB overall system efficiency.

The model performance was demonstrated by a hybrid micro-grid system [19]. The dynamic internal parameters of VRFB was extracted and flow rate was optimized considering both stack loss and pump loss simultaneously in the work of Bhattacharjee et al. [20]. The necessity of dynamic impedance matching between solar PV source and VRFB while designing efficient battery management system (BMS) was reported in their paper. The performance analysis of VRFB in photovoltaic micro grid was addressed by Nguyen et al. [21]. Qiu et al. [22] described the field validated model of VRFB for microgrid application. Turkar et al. [23] introduced a VRFB model for large scale applications. Hosseina et al. [24] discussed an optimal scheduling for distribution network with redox flow battery storage to satisfy the peak shaving, load levelling etc. Turkar et al. [25] described the utilization of VRFB to avoid wind power fluctuation penalties in an electricity market. Considering these practical applications, BMS for VRFB is very much essential for its efficient interfacing with renewable energy sources. Design of a proper charge controller [26] is one of the crucial requirements of an efficient BMS for on-grid and off-grid solar PV, wind power applications. Karami et al. [27] demonstrated the analysis and implementation of an adaptive PV based battery floating charger. Considering the intermittency

* Corresponding author.

E-mail address: ankurbhattacharjee@gmail.com (A. Bhattacharjee).

Nomenclature	
SOC	state of charge
I_{stack}	stack current (A)
Q	electrolyte flow rate ($\text{cm}^3 \text{s}^{-1}$)
N	electrolyte capacity (A s cm^{-3})
n_e	no. of electrons transferred per mole
F	Faraday's constant (96,485 C mol $^{-1}$)
c	vanadium concentration (mol L $^{-1}$)
$P_{pump_electrical}$	pump electrical power consumption (W)
η_{pump}	pump efficiency
R	universal gas constant ($8.3144 \text{ J K}^{-1} \text{ mol}^{-1}$)
T	ambient temperature (K)
k	proportionality constant
$E_{Stack(OCV)}$	VRFB stack open circuit voltage (V)
n	no. of series cells in VRFB stack
$E_{Cell_eq(at50\%SOC)}$	VRFB cell equilibrium potential (V)
$I_{parasitic}$	parasitic current (A)
R_P	parasitic resistance (Ω)
R_0	electrolyte solution resistance inside the stack (Ω)
R_{ct}	charge transfer resistance inside the stack (Ω)
C_{dl}	double layer capacitor (F)
I_d	diffusion current (A)
C_i	concentration of vanadium species (mol L $^{-1}$)
D_m	diffusion coefficient ($\text{m}^2 \text{s}^{-1}$)
x	thickness of the membrane (μm)
$E_{self_discharge}$	self discharge potential drop (V)
$R_{self_discharge}$	self discharge resistance (Ω)
E^+	positive electrode potential (V)
E^-	negative electrode potential (V)
E_+^0	positive electrode equilibrium potential (V)
E_-^0	negative electrode equilibrium potential (V)
C_O^+	concentration of oxidized vanadium species in the positive electrolyte side (mol L $^{-1}$)
C_O^-	concentration of oxidized vanadium species in the negative electrolyte side (mol L $^{-1}$)
C_R^+	concentration of reduced vanadium species in the positive electrolyte side (mol L $^{-1}$)
C_R^-	concentration of reduced vanadium species in the negative electrolyte side (mol L $^{-1}$)
E_{stack}	VRFB Stack terminal voltage (V)
i_{charge}	charging current (A)
$i_{discharge}$	discharging current (A)
η_{max}	maximum VRFB overall system efficiency
P_{Charge}	power consumed by VRFB during charging power (W)
$P_{Discharge}$	power delivered by VRFB during discharging (W)
P_{stack}	power inside the VRFB stack (W)
P_{int_loss}	power lost due to VRFB stack internal resistance (W)
$\eta_{charging}$	VRFB charging efficiency
K	permeability of porous electrode (m^2)
μ	dynamic viscosity of the electrolyte (Pa s)
Δp_{stack}	pressure drop across the stack (Pa)
Δp_{pipe}	pressure drop due to pipes (Pa)
P	density of the electrolyte (kg m^{-3})
V_s	velocity of the electrolyte inside the pipe (m s^{-1})
Z	height of the pipe (m)
G	acceleration due to gravity (m s^{-2})
h_m	minor losses (m)
h_f	friction losses (m)
f	Friction factor
L	length of pipe (m)
D	hydraulic diameter of the pipe (m)
Re	Reynolds' number

and low efficiency of solar PV source, the maximum power point tracking (MPPT) [28–30] technique needs to be applied for improved power conversion while charging the battery storage from solar PV source. The literatures [31–33] described the design and performance of solar MPPT based battery charge controller. The power converters play significant role in efficient conversion of solar PV power to the battery and the load/grid. Fathabadi et al. [34,35] demonstrated a high efficiency DC-DC boost converter based solar PV battery charge controller performance. A dc-dc buck converter operation and control for stand-alone solar battery charge controller was discussed by López et al. [36]. Nguyen et al. [37] proposed a low cost and fast charging topology for solar vehicle applications. With an emphasis on solar PV charge controller, it may be noted that the voltage excursion/cell in VRFB is about 38% as compared to that of same capacity lead acid battery which is about 20%. Thus the role of MPPT in VRFB charging is more important than lead acid or similar battery storage systems. VRFB has a wider range of cell voltage (1–1.6 V/cell) as compared to lead acid (1.95–2.4 V/cell) batteries and therefore it is more attractive to apply MPPT while charging VRFB from solar PV source. For a 48 V lead acid battery the voltage range is 46.8–54.4 V which is equivalent to a 34 cell VRFB stack. Therefore the voltage range for the equivalent VRFB system becomes 34–54.4 V which demands much more application of MPPT algorithm for its interfacing with solar PV source for avoiding loss of solar PV power. Unlike the other conventional batteries like lead acid, Li-ion, etc. the major challenge in designing efficient charge controller for VRFB is its simultaneous control of charging current and flow rate to achieve the maximum VRFB overall system efficiency besides improved charging efficiency. For fast charging operations of VRFB, the high current cause excessive rise in temperature inside VRFB stack which may lead to premature thermal shut down of the charging system in order to maintain safe operation of VRFB. It may be noted

that VRFB suffers from thermal precipitation at a temperature above 40 °C as reported by Tang et al. [38] and Yan et al. [39]. Hence the flow rate needs to be dynamically optimized [40–42] in order to overcome the problem of stack temperature rise beyond safe limit and incomplete charging.

In this paper a real time flow control based solar PV MPPT charge controller for VRFB system has been developed and its performance is demonstrated under dynamic solar irradiance profiles. The charging power conditioning unit is the DC-DC buck converter designed for efficient interfacing VRFB with solar PV source. Three different charging algorithms are implemented on the developed charging system using dsPIC (dsPIC33FJ32MC204) controller platform and their performances are compared. Besides the MPPT based CC-CV charging topology for maximizing the charging efficiency, the real time control of flow rate is also incorporated in the charging algorithm in order to achieve maximum VRFB overall system efficiency and controlled temperature rise inside the VRFB stack. The modified charging topology also prevents the possibility of premature thermal shut down of the charge controller due to temperature rise beyond 40 °C and hence ensures complete charging of VRFB. The performance of the charge control algorithm is validated by a 1 kW 6 h VRFB system. The proposed controller is a generalised one and thus very useful for large scale VRFB systems in solar PV applications.

Rest of the paper is organised as follows, Section 2 gives a schematic description of the proposed solar PV charge controller for VRFB system. Section 3 discusses the modelling and simulation of different subsystems of the proposed VRFB charge controller. In Section 4, the design of experimental set up and different subsystems have been described. The model performance and experimental results with two practical case studies are shown in Section 5. Finally, Section 6 includes the conclusion of this paper.

2. Proposed system topology

The schematic of the overall system topology for the proposed real time flow control integrated solar PV MPPT charge controller of VRFB is shown in Fig. 1. The control switches SW1, SW2 are used for charging and SW3, SW4 are used for discharging experiments. The DC-DC converter module is designed for efficient power transfer from the solar PV to VRFB. The DC-AC converter is designed to control the two single phase AC pumps to maintain dynamic flow rates under different charging conditions [42]. The charging algorithms and real time pump control logic are implemented by a 16-bit dsPIC microcontroller (dsPIC33FJ32MC204) acting as the central processor unit.

3. Simulation and modelling

As shown in Fig. 1, the proposed VRFB charge controller is designed and simulated in MATLAB/Simulink platform to ensure proper selection of the control parameter values and the converter circuit elements.

3.1. VRFB system modelling

Development of an efficient charge controller for VRFB requires accurate estimation of its stack terminal voltage under dynamic charging and discharging current with real time flow rate control. Therefore a dynamic equivalent model of VRFB system in MATLAB/Simulink environment described in the paper of Bhattacharjee et al. [18] is further modified and utilized in this paper as shown in Fig. 2a. Besides the accurate estimation of VRFB stack terminal voltage for charge controller application, another major role of this electrical equivalent circuit model of VRFB is the impedance matching among the solar PV source, VRFB and the grid/load for transferring maximum power in the network as shown in Fig. 2b.

The design parameters for modelling the VRFB system and the proposed real time flow control integrated solar PV MPPT charge controller is shown in Table 1.

This model is used to determine accurate stack terminal voltage of VRFB during charging and discharging operations considering the impact of practical parameters like flow rate, SOC and self discharge drop etc. In this work the impact of shunt current (I_{sh}) due to the guide and manifold channels in the VRFB stack is neglected because of its negligibly small magnitude within 1% of the terminal current as reported by Zhang et al. [17].

From the Nernst potential equation and considering the effect of self discharge loss, the VRFB stack open circuit voltage (OCV) is determined

by Eq. (1).

$$E_{stack(OCV)}(t) = n \times \left\{ E_{Cell_eq(at50\%SOC)} + \frac{2RT}{F} \ln\left(\frac{SOC}{1-SOC}\right) - I_d R_{self_discharge}(t) \right\} \quad (1)$$

where

$$\begin{aligned} E_{stack(OCV)} &= \text{VRFB stack open circuit voltage (V)} \\ E_{Cell_eq(at50\%SOC)} &= \text{VRFB cell equilibrium potential (V)} \\ n &= \text{No. of series cells in VRFB stack} \\ R &= \text{Universal gas constant (8.3144 J K}^{-1} \text{ mol}^{-1}) \\ T &= \text{Ambient temperature (K)} \\ F &= \text{Faraday's constant (96,485 C mol}^{-1}) \\ I_d &= \text{Diffusion current (A)} \\ R_{self_discharge} &= \text{Self discharge equivalent resistance (\Omega)} \end{aligned}$$

For accurate estimation of VRFB stack OCV, the self discharge potential drop is determined by using the equations developed by Bhattacharjee et al. [18]. In their paper, the self discharge loss is considered as the potential drop caused by diffusion of vanadium ions through the proton exchange membrane from both positive and negative electrolyte sides even when the VRFB is kept under open circuit condition over a period of time. The self discharge loss calculated in their work is basically the SOC drop represented by the corresponding voltage drop which is a practical phenomenon of VRFB. However, to represent the dissipative self discharge loss in the MATLAB based electrical equivalent circuit model of VRFB, it is necessary to introduce equivalent resistive unit that accounts for the same dissipative loss although physically no such resistance appears inside the battery stack. Therefore estimation of the diffusion current and an equivalent resistance ($R_{self_discharge}$) is very essential to validate the impact of self discharge on the VRFB OCV. The diffusion current is a function of the concentration gradient ($\frac{dc_i}{dx}$) and diffusion coefficients (D_m) of different vanadium species from two half cells at a certain initial SOC. The diffusion current is calculated by Eq. (2);

$$I_d = C_i D_m \frac{dc_i}{dx} \quad (2)$$

where

$$\begin{aligned} I_d &= \text{Diffusion Current (A)} \\ C_i &= \text{Concentration of Vanadium Species (mol L}^{-1}) \\ D_m &= \text{Diffusion coefficient (m}^2 \text{s}^{-1}) \end{aligned}$$

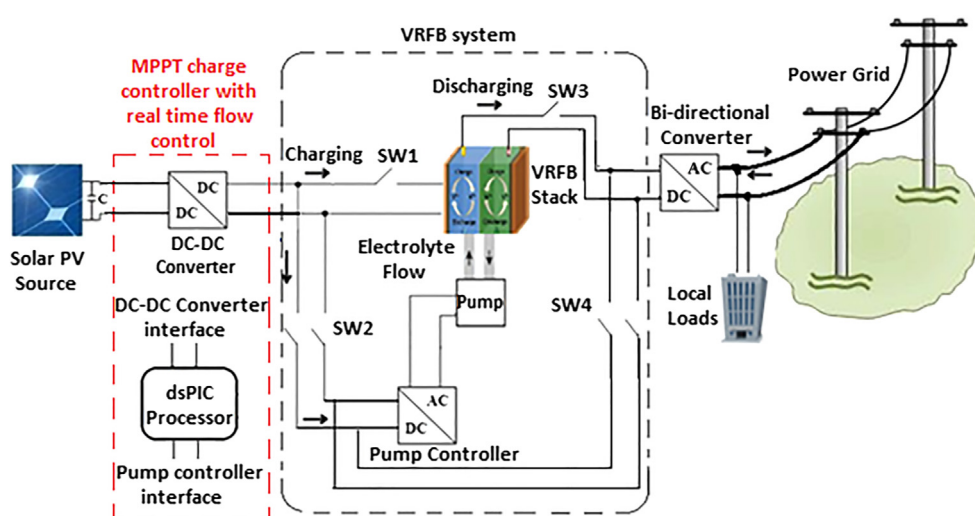


Fig. 1. Block diagram representation of the experimental configuration for the proposed solar PV MPPT based VRFB charge controller.

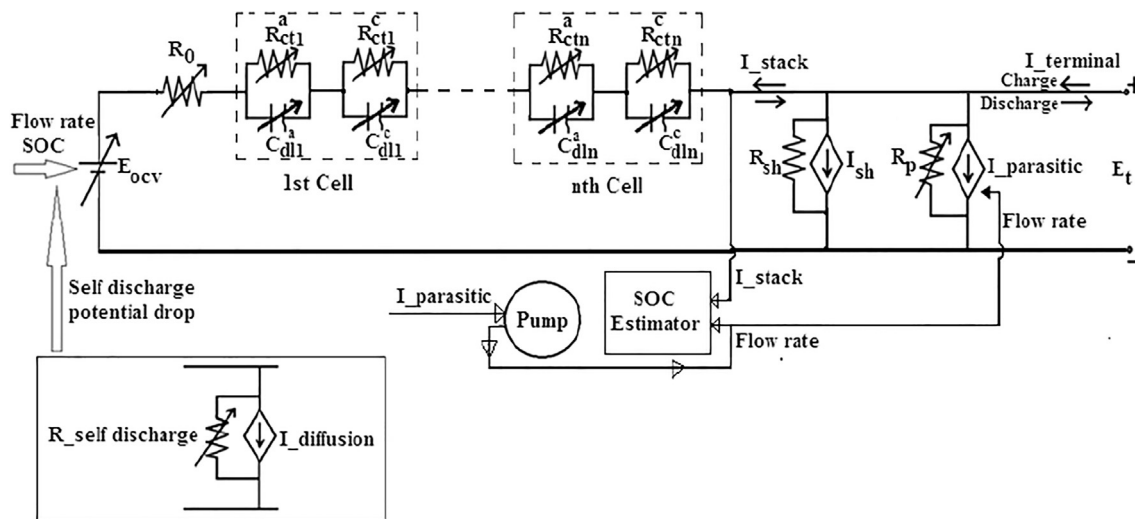


Fig. 2a. Schematic of VRFB system electrical equivalent circuit [20].

x = Thickness of the membrane (μm)

The average concentration change (mol L^{-1}) of different vanadium ions from the experimental results and observations of You et al. [43] and Sun et al. [44] have been used to estimate diffusion current (I_d) for each vanadium ion while crossover through ion exchange membrane.

The open circuit voltage (OCV) drop during self discharge is estimated from the basic Nernst potential equation considering the diffusion concentrations of vanadium species in half cells.

$$E^+(t) = E_+^0 + \frac{RT}{F} \ln \left(\frac{C_O^+(t)}{C_R^+(t)} \right) \quad (3)$$

$$E^-(t) = E_-^0 + \frac{RT}{F} \ln \left(\frac{C_O^-(t)}{C_R^-(t)} \right) \quad (4)$$

where

E^+ = Positive electrode potential (V)

E^- = Negative electrode potential (V)

E_+^0 = Positive electrode equilibrium potential (V)

E_-^0 = Negative electrode equilibrium potential (V)

C_O^+ = Concentration of oxidized vanadium species in the positive electrolyte side (mol L^{-1})

C_O^- = Concentration of oxidized vanadium species in the negative electrolyte side (mol L^{-1})

C_R^+ = Concentration of reduced vanadium species in the positive electrolyte side (mol L^{-1})

C_R^- = Concentration of reduced vanadium species in the negative electrolyte side (mol L^{-1})

Table 1

Design parameters for modelling the VRFB system and the proposed solar PV MPPT charge controller.

Parameters	Quantity	Unit
No. of VRFB cells in stack	20	–
Vanadium concentration (c_v)	1.6	Mol L^{-1}
Volume of electrolyte in each tank	180	L
No. of electron transferred/mol (n_e)	1	–
Dimension of each electrode ($L_{felt} \times W_{felt} \times D_{felt}$)	25 × 25 × 0.3	$\text{cm} \times \text{cm} \times \text{cm}$
Inner diameter of the flow pipe	18	cm
Inner diameter of the guide channel	5	cm
Length of the guide channel	117	cm
Inner diameter of the manifold	7.5	cm
Length of the manifold	42	cm
VRFB power capacity	1	kW
VRFB energy capacity	6	kWh
VRFB stack voltage range	20–32	V
VRFB equilibrium potential	28	V
Rated Ah capacity	187	Ah
Stack temperature variation	29–31	°C
Pump rated power ($\times 2$)	85($\times 2$)	W
Pump rated voltage (AC)	220	V
Pump rated current	0.5	A
Solar PV array power capacity	2	kW_P
PV side capacitor rating	470($\times 4$)	μF
Maximum DC-DC converter efficiency	96%	–
DC-DC converter switching (IGBT) frequency	20	kHz
DC-DC converter output filter capacitor rating	2200($\times 2$)	μF
DC-DC converter output filter inductor rating	150	μH
Filter inductor R.M.S current	62	A
Filter inductor saturation current	80	A

$$E_{selfdischarge}(t) = E^+(t) - E^-(t) \quad (5)$$

Then the net potential during self discharge becomes,

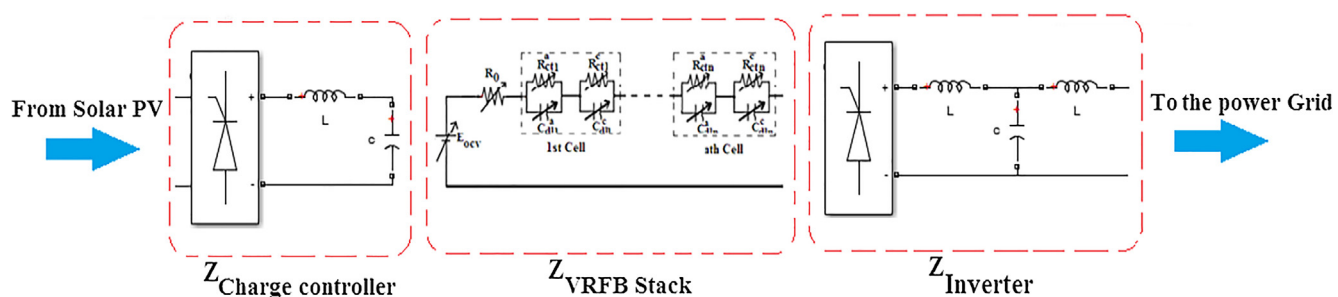


Fig. 2b. Impedance matching for transferring maximum power from the solar PV source to VRFB and to the load/grid [20].

The self discharge equivalent resistance ($R_{self_discharge}$) is estimated by the diffusion current (I_d) and Nernst potential during crossover of vanadium species and presented by Eq. (6).

$$R_{self_discharge}(t) = \frac{E_{self_discharge}(t)}{I_d(t)} \quad (6)$$

$R_{self_discharge}$ is a variable parameter which varies with the change in concentration of different vanadium species while cross over through membrane under open circuit condition over a period of time. But it is independent of charging and discharging current as the diffusion process considered in this work is under open circuit condition.

The VRFB stack terminal voltage is estimated by Eq. (7).

$$E_t(t) = E_{stack(OCV)}(t) \pm I_{stack} R_{int}(Q, I) \quad (7)$$

where

E_t = VRFB stack terminal voltage (V)

I_{stack} = VRFB stack terminal current (A)

R_{int} = VRFB stack internal resistance (Ω)

Q = Electrolyte flow rate (ml/s)

I = VRFB stack current (A)

In Eq. (7), the '+' sign signifies the charging and '-' sign signifies discharging condition. R_{int} is a function of flow rate (Q) and stack current (I) as reported by Zhang et al. [17]. However, for simplicity of modelling, R_{int} is considered as constant value of $0.03\ \Omega$ considering its small variation in ' $m\Omega$ ' range with flow rate and stack current.

Considering the pressure drop in the electrolyte flow pipes and stack of the VRFB system, head loss and the mechanical power consumption of the flow pumps are calculated based on the hydraulic equations reported by Zhang et al. [17] as the stack and the channel dimensions of the VRFB system used in this work is similar to their work.

Majority of the pressure drop arise due to the VRFB stack. It is reported that nearly 70% of this pressure loss is observed inside the felt electrodes [16]. The felt electrode can be considered of as a porous sponge and the hydraulic resistance ($\tilde{R}_{half\ cell}$) offered by is estimated by the Darcy equation as shown in Eq. (8) [16,17]

$$\tilde{R}_{half\ cell} = \frac{\mu L_{felt}}{k W_{felt} D_{felt}} \quad (8)$$

where

k = permeability of porous electrode

μ = dynamic viscosity of the electrolyte.

The total pressure drop of VRFB stack is equal to that of a single cell, because the electrolyte flows parallel through each cell inside the stack. The total pressure drop in the stack is obtained by Eq. (9) [17],

$$\Delta p_{stack} = 2 \times \frac{Q \tilde{R}_{half\ cell}}{0.7n} \quad (9)$$

The pressure drop from the pipes in the external circuit also contributes significantly to the total pressure loss of the system. The pressure drop inside the pipe is modelled using the extended Bernoulli's equation (10) [17],

$$\Delta p_{pipe} = -\rho g \left(\frac{\Delta V_s^2}{2g} + \Delta z + h_f + h_m \right) \quad (10)$$

where

ρ = density of the electrolyte

V_s = Velocity of the electrolyte inside the pipe

z = height of the pipe.

g = acceleration due to gravity.

Table 2
Loss coefficients for minor losses [14].

Geometry	Loss coefficient K_l
From a reservoir into a pipe	0.04–0.9
From a pipe into a reservoir	1
Bends and elbows	0.2–1.5
Valves	0.15–10

The minor losses (h_m) are given by Eq. (11) [16,17],

$$h_m = K_l \frac{\Delta V_s^2}{2g} \quad (11)$$

where

K_l = Loss co-efficient.

The different values of K_l used to model are provided in Table 2.

The friction losses (h_f) due to flow inside the pipe is given by the Darcy–Weisbach equation as shown in Eq. (12) [17],

$$h_f = f \frac{L}{D} \frac{\Delta V_s^2}{2g} \quad (12)$$

where

f = friction factor

L = Length of pipe

D = Hydraulic diameter of the pipe

The friction factor (f) is dependent on the type of flow. In order to determine the nature of flow through the pipe, i.e. laminar or turbulent, the Reynolds number (Re) is calculated by Eq. (13),

$$Re = \frac{\rho V_s D}{\mu} \quad (13)$$

Depending on the Reynolds' number, the friction factor (f) is computed as,

$$f = \frac{64}{Re}, \quad Re < 2000 \quad (14)$$

And

$$f = 0.316 Re^{-0.25}, \quad 4000 < Re < 10,000 \quad (15)$$

Once the total pressure drop is calculated, the hydraulic power required by the pumps is given by the following equation,

$$P_{hydraulic} = Q(\Delta p_{stack} + \Delta p_{pipe}) \quad (16)$$

The pump electrical power consumption has been estimated considering the pump efficiency characteristics curve shown by Li et al. [38]. The pump electrical power is calculated by Eq. (17) [18],

$$P_{pump_electrical} = \frac{P_{pump_hydraulic}}{\eta_{pump}} \quad (17)$$

where

$P_{pump_electrical}$ = Pump electrical power consumption (W)

$P_{pump_hydraulic}$ = Pump hydraulic power consumption (W)

η_{pump} = Pump efficiency

3.2. Solar PV VRFB charging algorithms

In this paper, three different solar charging topologies for VRFB have been simulated in MATLAB/Simulink environment and the results are validated by experimental results. The performances of the three algorithms are compared. The charging efficiency is calculated by Eq.

(18);

$$\text{The charging efficiency } \eta_{\text{charging}} = \frac{P_{\text{VRFB}}}{P_{\text{PV}}} \quad (18)$$

where

 P_{VRFB} = Charging power supplied to the VRFB stack (W) P_{PV} = Solar PV output power (W)

Unlike the other conventional batteries, it is to be noted that the solar PV charging algorithms for VRFB consist of real time flow rate control in conjunction with the charging current control loop.

3.2.1. Real time flow control integrated MPPT charging of VRFB

In this topology, the maximum power is extracted from the solar PV source under varying irradiance and VRFB is charged with maximum charging efficiency. A simple perturb & observe (P&O) [28] algorithm is adopted to track the maximum power point (MPP) from solar PV output as shown in Fig. 3a. A real time flow rate optimization (Q_{opt}) is incorporated with dynamic SOC variation to achieve maximum VRFB overall system efficiency (η_{max}) and to control the temperature rise inside the VRFB stack. As shown in the flow chart of the MPPT charging algorithm in Fig. 3b, the VRFB stack temperature is controlled within the predefined threshold of ' T_{max} ' which is 40 °C [38,39] by real time control of flow rate with a step of ' ΔQ ' (10 ml/s). In order to save the VRFB from over potential problem, the charging algorithm is such designed that it stops charging once the VRFB terminal voltage reaches the overcharge limit (V_{oc}). A suitable DC-DC buck converter is designed to execute the MPPT charging for VRFB under dynamic irradiance profile.

3.2.2. Real time flow control integrated solar PV three stage CC - CV charging of VRFB

The three stage charging methodology is described by the flow chart shown in Fig. 4. In this charging topology, two constant current modes are applied followed by a constant voltage mode. At the initial stage, a small constant current of C/10 (Trickle current) is supplied to the VRFB until the battery voltage reaches a predefined threshold called trickle

voltage (V_{Trickle}). This charging stage is termed as trickle charging stage. The reason of supplying a small current at the initial stage of charging is to reduce excessive heat generation inside the battery stack and side reaction. In the second stage of charging, a high current of C/3 (Bulk current) is supplied to the battery until the battery voltage reaches its overcharging limit (V_{oc}). This stage of charging is termed as bulk charging which helps in fast charging of VRFB. The third stage of charging involves a constant voltage mode where the V_{oc} is maintained across the VRFB stack terminal till its charging current is reduced to a very low level of C/100 (Float current) which ensures complete charging of battery. This charging stage is termed as float charging stage. The term "C" is the Ah capacity of VRFB. Like the MPPT charging algorithm shown in Fig. 3, the real time flow rate control is also implemented along with the current control loop in order to achieve maximum VRFB overall system efficiency and control of VRFB stack temperature within the safe operating limit to avoid premature thermal shut down of the charge controller.

3.2.3. Modified three stage solar PV charging of VRFB

Although the aforesaid three stage CC-CV charging topology can ensure safe and complete charging of VRFB but it is also essential to improve the charging efficiency especially for the intermittent power source like solar PV. Therefore, a modified three stage charging topology is adopted as shown in the flow chart in Fig. 5. In this charging topology, the maximum power point (MPP) is tracked by the charge controller from solar PV source under dynamic solar insolation and the current at maximum power point (I_{MPP}) is fed to the VRFB stack in the bulk charging phase. This enhances the power transfer from solar PV to the VRFB and thus improving the charging efficiency. Hence in the modified three stage charging topology, the charging of VRFB ensures safe, complete and efficient charging for solar PV applications. The dynamic optimal flow rate (Q_{opt}) is also incorporated in the proposed algorithm to overcome the problem of premature thermal shut down of the controller due to rise in VRFB stack temperature beyond its safe limit of operation and thus ensuring complete charging.

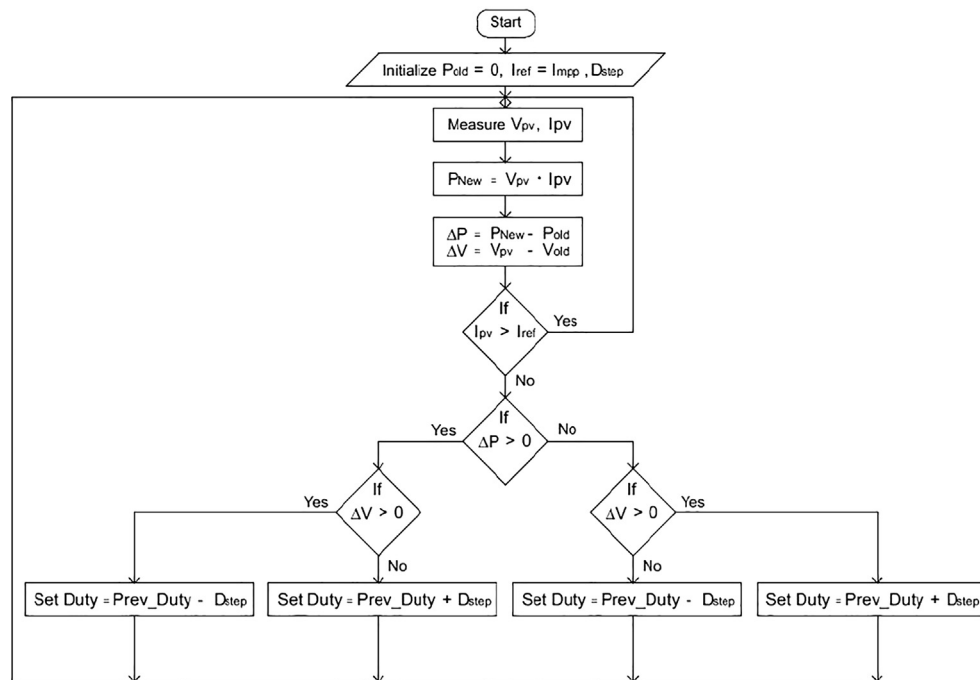


Fig. 3a. Flow chart of the Perturb & Observe (P&O) MPPT algorithm.

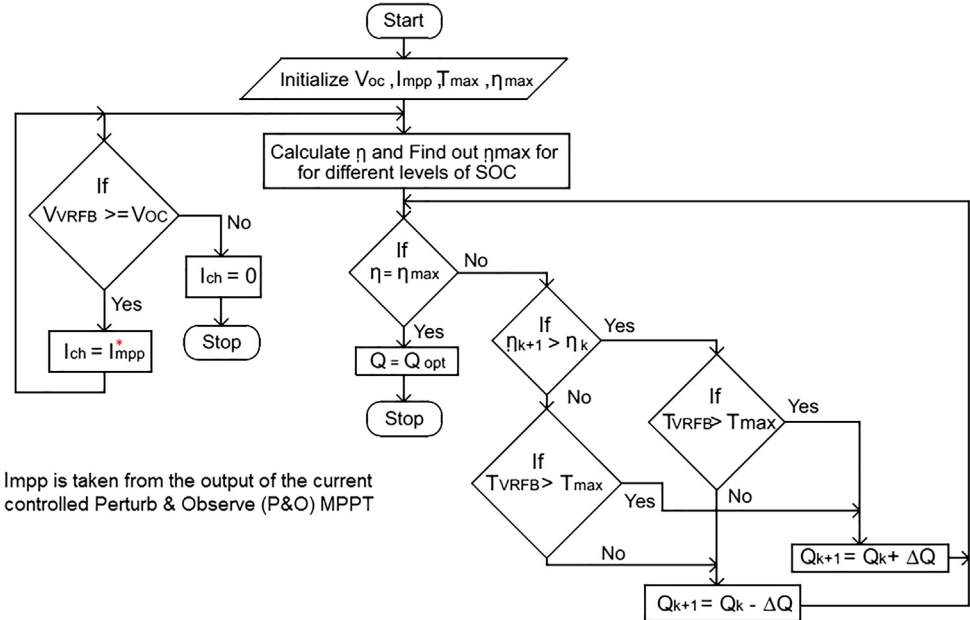


Fig. 3b. Flow chart for the real time flow control integrated MPPT charging of VRFB.

3.3. Dynamic flow rate optimization

In order to improve the VRFB overall system efficiency, the power consumed by flow pumps needs to be optimized. While maintaining different levels of charging current to the VRFB for solar PV applications, the flow rate also varies with the SOC. In the paper of Bhattacharjee et al. [18] the dynamic range of optimal flow rate has

been estimated for 1 kW 6 h VRFB system thus the overall VRFB system efficiency has been improved. Based on that work, in this paper the dynamic optimal flow rate is identified for the VRFB system under different charging condition to optimize the pump power loss and to improve the VRFB system efficiency. The optimal flow rate control algorithm is validated by 1 kW 6 h VRFB system with three stage CC-CV solar MPPT charging experiment. It is to be noted that the total

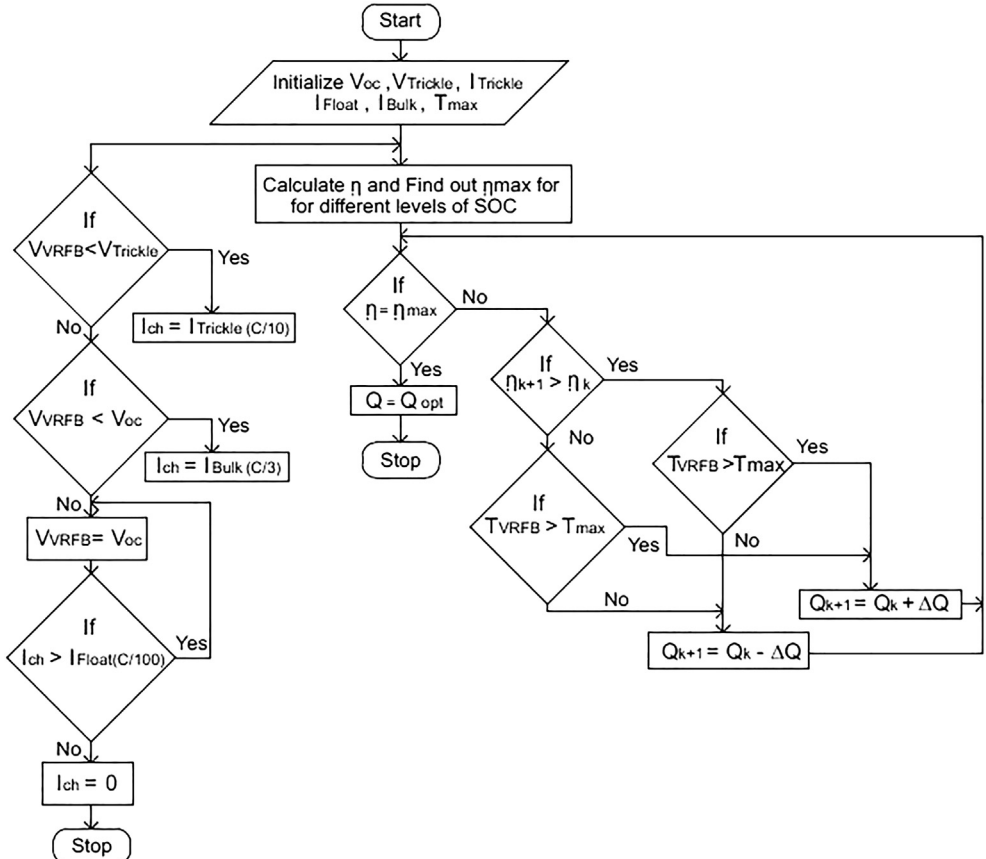


Fig. 4. Flow chart for the real time flow control integrated three stage CC-CV solar charging of VRFB.

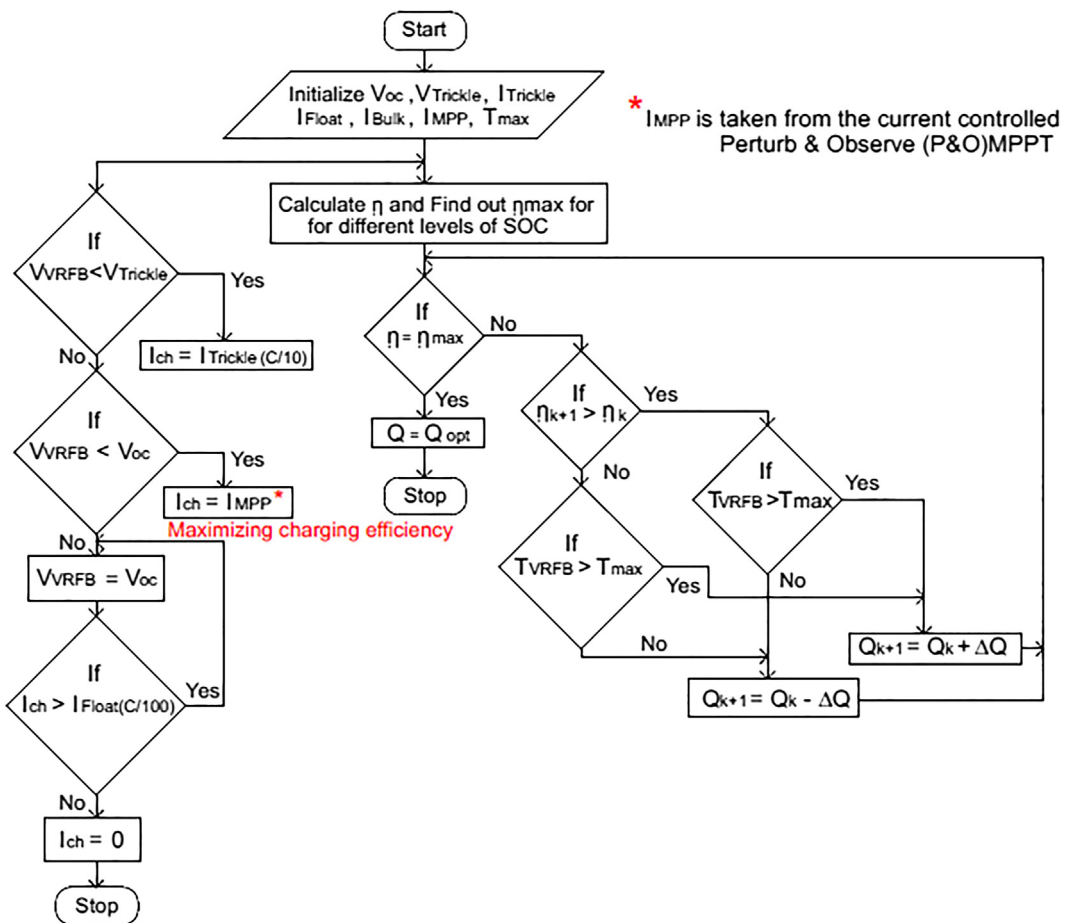


Fig. 5. Flow chart for real time flow control integrated MPPT based CC-CV charge controller for VRFB.

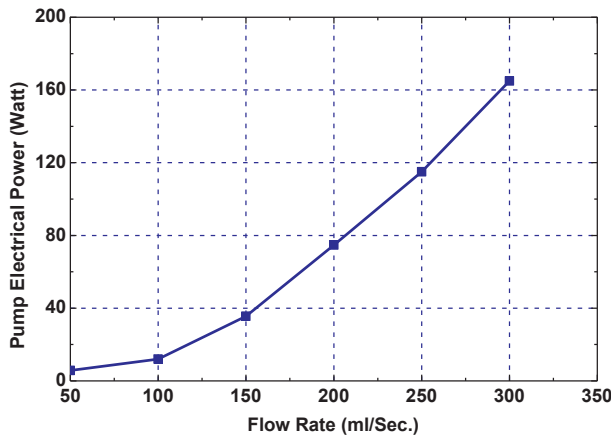


Fig. 6. Pump electrical power consumption under different flow rates [18].

charging power for the VRFB system is the sum of the power consumed by the VRFB stack and the pumps as shown in Eq. (19). The pump power (P_{pump}) increases exponentially with flow rate (Q) and has significant contribution in the overall power consumption of VRFB. Similarly, the effective discharging power of VRFB is calculated by Eq. (20). The stack power (P_{stack}) is the product of the stack terminal voltage and the current, expressed by Eq. (21). Eq. (22) depicts the VRFB stack internal power loss (P_{int_loss}).

$$P_{Charging} = (P_{stack} + P_{int_loss} + P_{pump}(Q)) \quad (19)$$

$$P_{Discharging} = (P_{stack} - P_{int_loss} - P_{pump}(Q)) \quad (20)$$

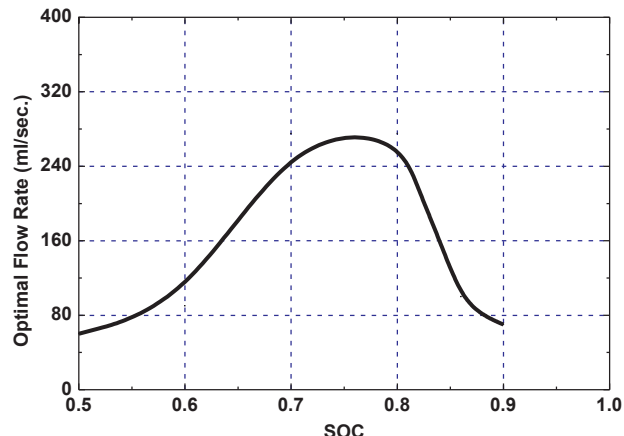


Fig. 7. Dynamic optimal flow rate for the three stage CC-CV solar MPPT charging for 1 kW 6 h VRFB.

Table 3

VRFB system efficiency corresponding to dynamic optimal flow rates over dynamic SOC range.

SOC (%)	Dynamic optimal flow rate (ml/s)	P_{min_charge} (W)	$P_{max_discharge}$ (W)	η_{max} (%)
50	60	942.7	842	89.31
60	120	967	858	88.72
70	240	1018	889	87.33
80	250	1059	922	87.06
90	70	930	825	88.70



Fig. 8a. The overall experimental configuration for the real time flow control based solar MPPT charge controller and BMS for 1 kW 6 h VRFB.

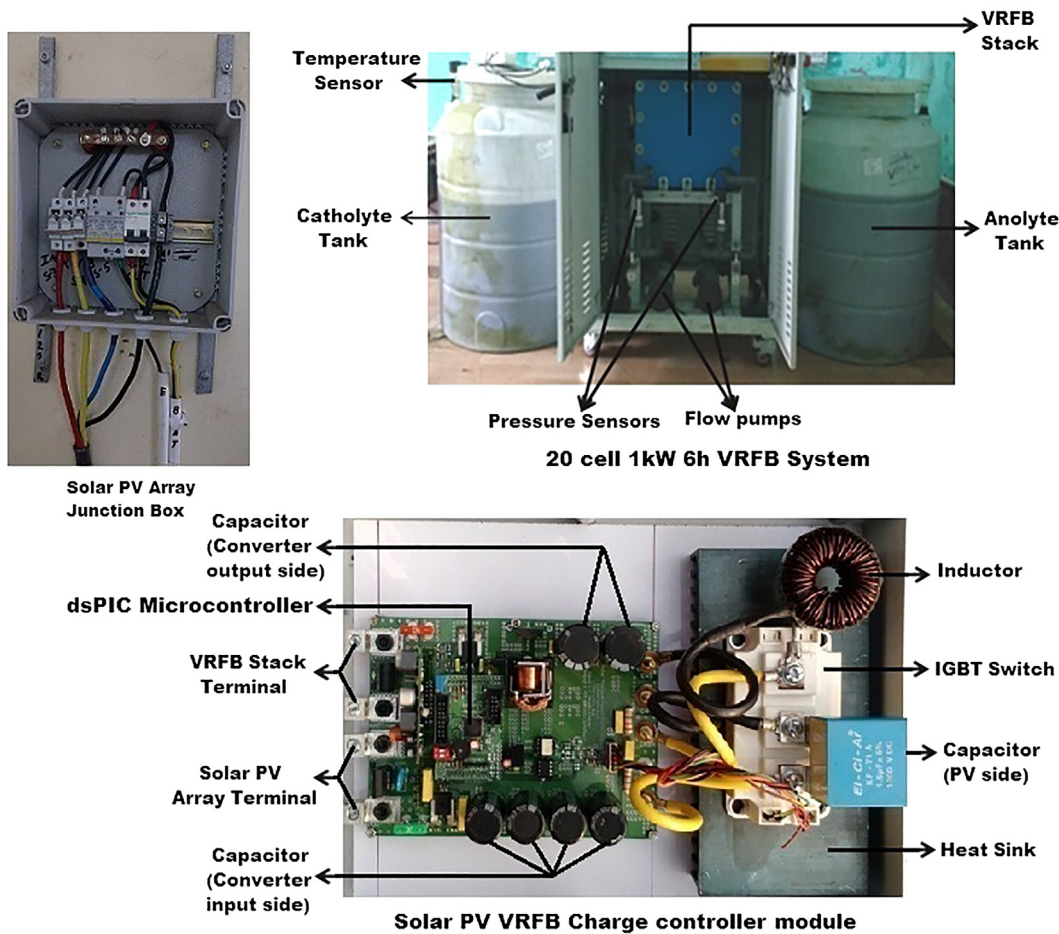


Fig. 8b. Zoomed in view of the individual subsystems of the experimental set up.

$$P_{stack} = V_t \times I_{stack} \quad (21)$$

$$P_{int_loss} = I_{stack}^2 \times R_{int} \quad (22)$$

where

$P_{Charging}$ = Total charging power consumed by the VRFB system (W)

$P_{Discharging}$ = Total discharging power delivered by the VRFB system (W)

P_{stack} = Power consumed by VRFB stack during charging (W)

P_{int_loss} = VRFB stack internal loss (W)

P_{pump} = Power consumed by the pumps (W)

V_t = VRFB stack terminal voltage (V)

I_{stack} = VRFB stack current (A)

R_{int} = VRFB stack internal resistance (Ω)

The power consumed by flow pumps corresponding to the dynamic

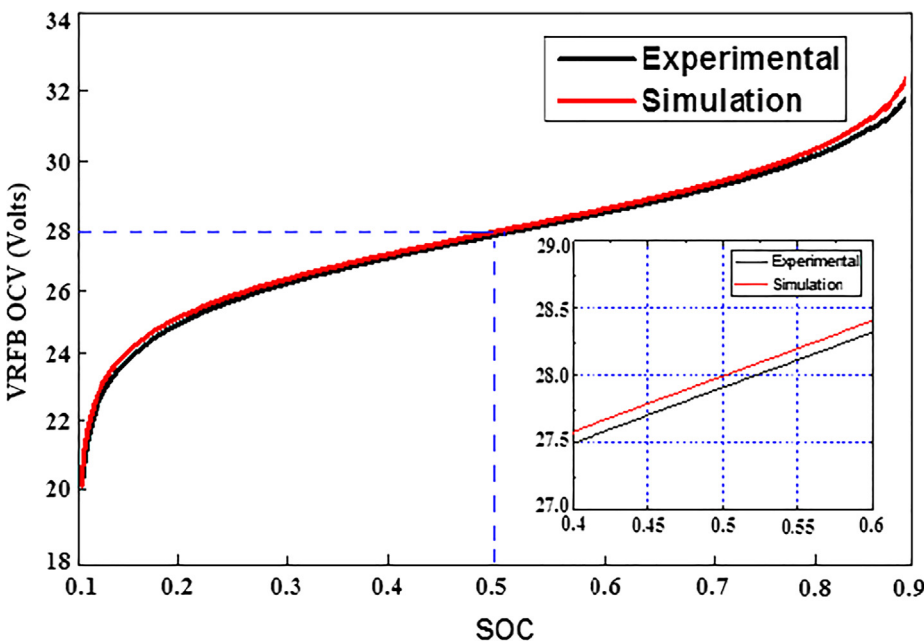


Fig. 9. Simulation and experimental validation of OCV-SOC characteristics of a 20 Cell VRFB (1–1.6 V/Cell) at 40 A constant current charging (At the inset the simulation and experimental OCV has been compared at 50% SOC) [18].

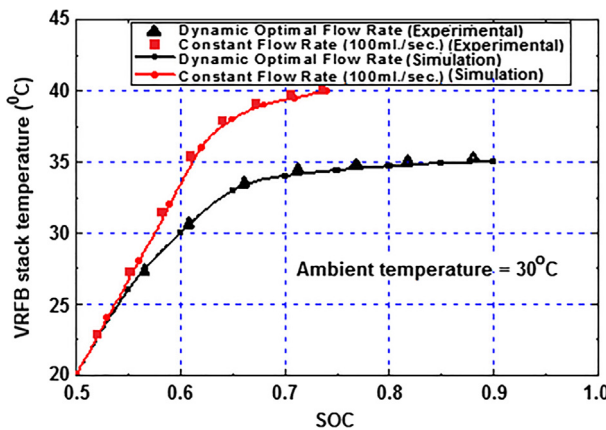


Fig. 10. Comparison between the charging performances at constant and dynamic optimal flow rate operation of VRFB.

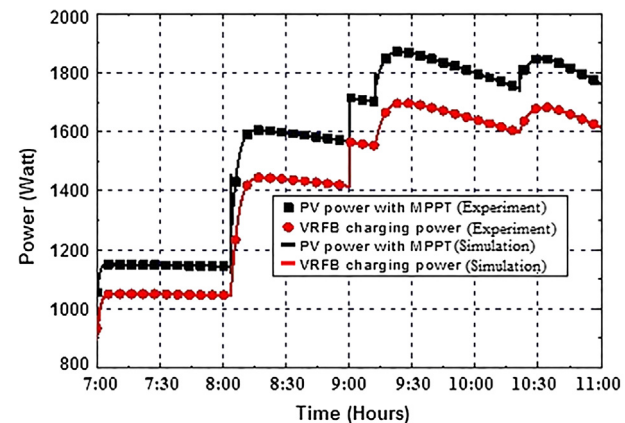


Fig. 12. Solar PV power and VRFB charging power with MPPT under dynamic insolation on a sunny day.

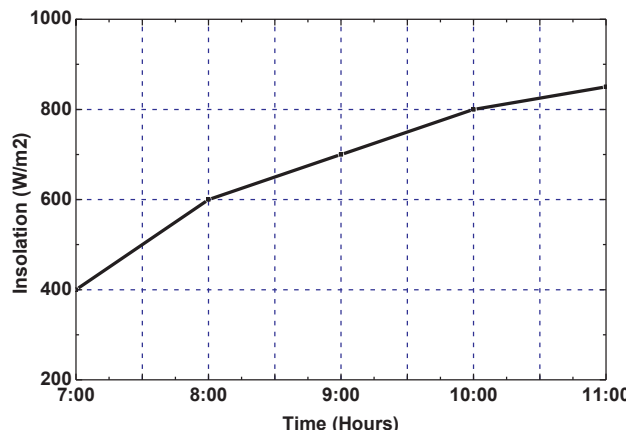


Fig. 11. Dynamic solar insolation profile on a sunny day (SRRA data taken from IIEST, Shibpur campus).

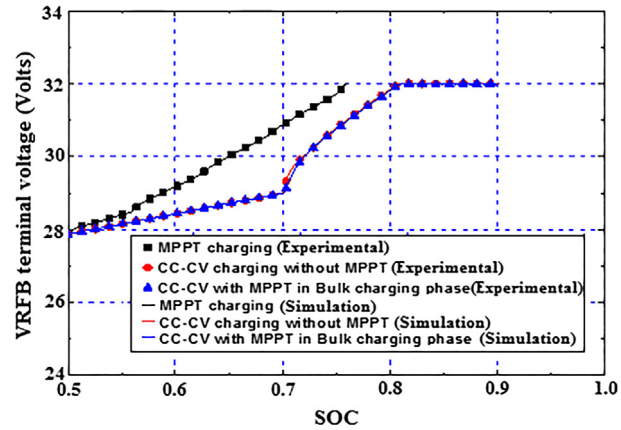


Fig. 13. VRFB terminal voltage for the three different solar charging topologies under sunny weather condition.

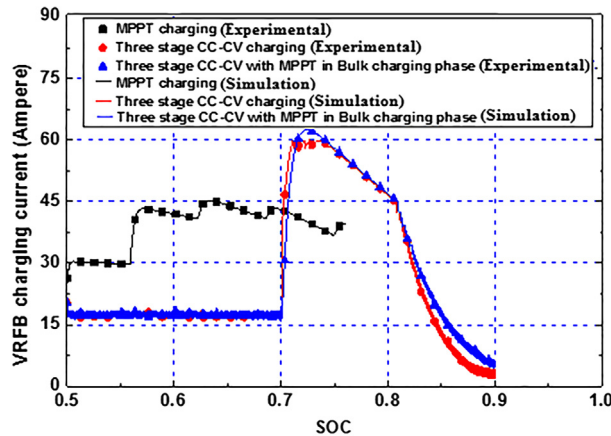


Fig. 14. VRFB charging current for the three different solar charging topologies under sunny weather condition (Simulation and experiments).

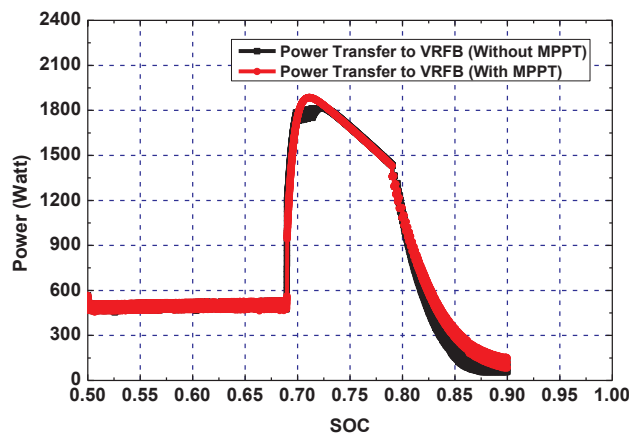


Fig. 15a. Comparison between the power transfer for three stage CC-CV charging with and without MPPT in the Bulk charging stage under sunny weather condition.

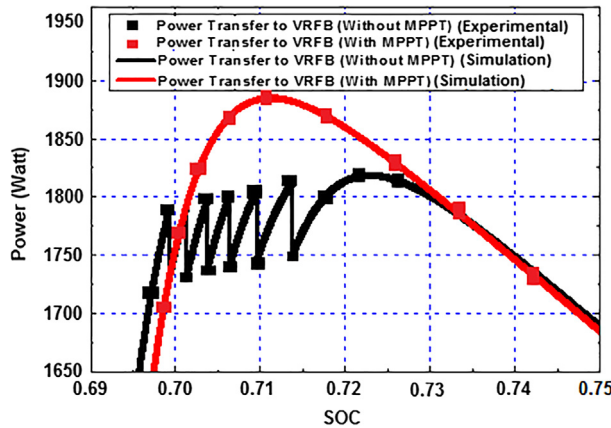


Fig. 15b. Zoomed in version of the VRFB charging power transfer for three stage charging without and with MPPT under sunny weather condition (Simulation & Experiments).

flow rates is shown in Fig. 6. The hydraulic power of the pump is converted into equivalent electrical power consumed by the pump based on the Eq. (17). The dynamic optimal flow rate is determined by finding out the minimum charging power (P_{charge_min}) and maximum discharging power ($P_{Discharge_max}$) of VRFB under dynamic current and load profile and thus maximizing the VRFB overall system efficiency. The overall system efficiency (η) of VRFB system is formulated by Eq.

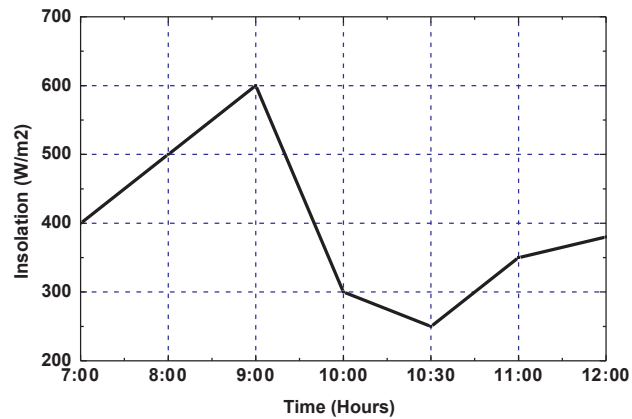


Fig. 16. Dynamic solar insolation profile under the appearance of cloud (SRRA data taken from IEST, Shibpur campus).

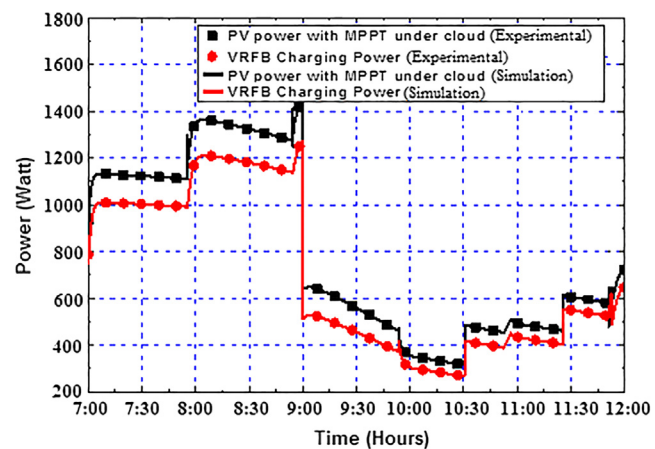


Fig. 17. Solar PV output power and VRFB charging power with MPPT under dynamic insolation and cloudy condition.

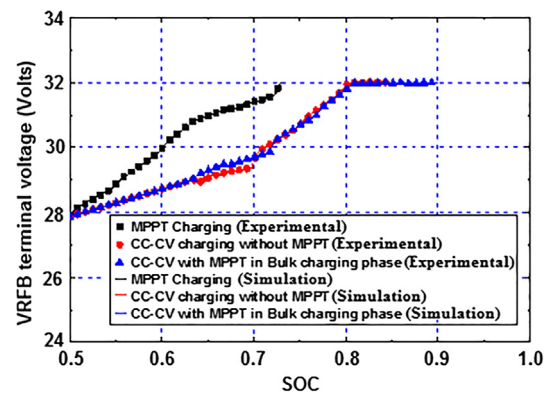


Fig. 18. VRFB terminal voltage at three different charging topologies under cloudy condition.

(23),

$$\eta = \frac{\int_0^{t_d} P_{Discharge}(t) dt}{\int_0^{t_c} P_{Charge}(t) dt} = \frac{\int_0^{t_d} (P_{stack} - P_{pump} - P_{int_loss}) dt}{\int_0^{t_c} (P_{stack} + P_{pump} + P_{int_loss}) dt} \quad (23)$$

As discussed in the flow charts in Figs. 3a, 4 and 5, besides the maximum VRFB overall system efficiency another important criterion for determining the dynamic optimal flow rate is controlling the rise in temperature inside VRFB stack which may lead to premature thermal

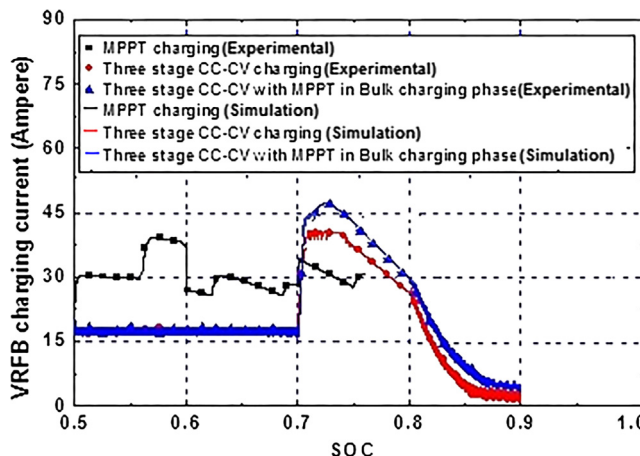


Fig. 19. VRFB charging current for the three different solar charging topologies under cloudy weather condition (Simulation and experiments).

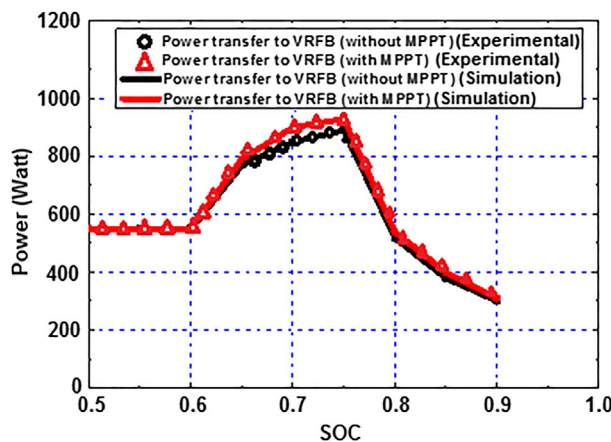


Fig. 20a. Comparison between the power transfer for three stage CC-CV charging with and without MPPT in Bulk charging stage under cloudy weather condition.

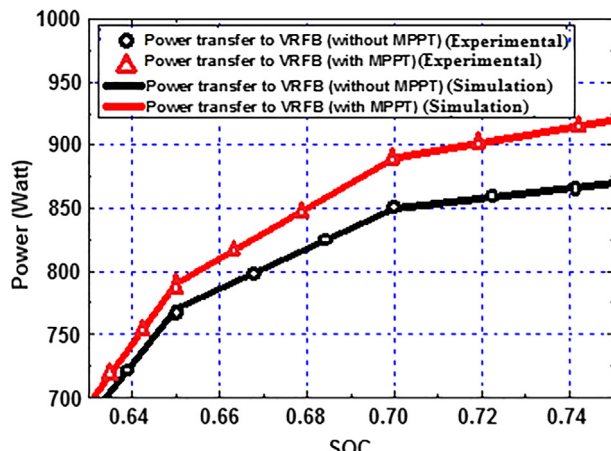


Fig. 20b. Zoomed in version of the VRFB charging power transfer for three stage charging without and with MPPT under cloudy weather condition.

shut down of the charging system in order to maintain safe operation of VRFB. This will further lead to incomplete charging of VRFB. The comparative analysis of the temperature rise inside the VRFB stack with constant flow and dynamic optimal flow is described in Section 5.1 in this paper. In Fig. 7, the dynamic optimal flow rate is determined over the range of SOC under MPPT enabled CC – CV charging from solar PV

source. The optimal flow rate range is found to be 60–250 ml/s for 1 kW 6 h VRFB system under dynamic charging current profile. It is observed from Fig. 7 that the typical SOC value starts from 50% which justifies the VRFB equilibrium potential of 28 V as mentioned in Eq. (1) shown in Section 3.1 of this paper.

The overall system efficiency of the 1 kW 6 h VRFB is obtained under dynamic current of three stage MPPT enabled charging and a constant discharging current of 30 A as shown in Table 3. The average of the maximum VRFB overall system efficiency is found to be around 88% which significantly higher compared to the reported data in the existing literatures [23,42].

4. Design of experimental set up

The overall experimental set up for validating the real time flow control integrated solar PV VRFB charging algorithms is shown in Fig. 8a. The major three subsystems of the proposed work are; solar PV array and its junction box, VRFB storage system and the charge controller module shown in Fig. 8b. For the 1 kW 6 h VRFB system, a solar PV array of 2 kW_P based on the daily average insolation in the locality. The DC-DC buck converter is designed to efficiently interface the 1 kW 6 h VRFB with 2 kW_P solar PV array. The converter module is first designed in MATLAB/Simulink environment and then fabricated based on the simulated values of those circuit elements. For controlling the flow rate in real time during different level of charging, a suitable DC-AC converter is also designed for speed control of the two pumps of VRFB system.

5. Result analysis and discussion

The performance of the charging algorithms described in Section 3.2 is demonstrated in simulation and experimental validation has been done. A 20 cell 1 kW 6 h VRFB system is charged from 2 kW_P solar PV source and suitable controller has been designed. Two practical insolation profiles have been used as input to the model and the three different charging algorithms are implemented in dsPIC processor. In this paper the model performance has been validated by two practical case studies. For designing proper charge controller the charging characteristics [18,20,45] VRFB is simulated and experimentally studied. It is found from Fig. 9 that the equilibrium potential of the 20 Cell 1 kW VRFB appears to be 28 V at 50% SOC with 1.4 V/cell and thus validating Eq. (1) as shown in this paper.

5.1. Importance of real time flow rate control for VRFB charge controller

Unlike the other conventional batteries like lead acid, Li-ion [46], etc. the real time monitoring and control of flow rate is crucial in case of designing the charge controller for VRFB. As described in Section 3.3 of this paper, the flow rate needs to be dynamically optimized not only to ensure maximum VRFB overall system efficiency but also to control the rise in temperature inside VRFB stack which may lead to premature thermal shut down of the charging system in order to maintain safe operation of VRFB. A comparison has been shown in Fig. 10 where it is observed that VRFB stack temperature rises up to 40 °C during charging at constant flow rate which leads to incomplete charging (SOC up to 74%) of VRFB due to thermal shut down of the charge controller for protection purpose. The predetermined upper threshold of stack temperature is set as 40 °C [38,39] by the controller for safe operation of VRFB system. This problem is mitigated by implementing dynamic optimal flow rate during charging where the stack temperature is kept within 35 °C and thus ensures complete charging of VRFB up to 90% SOC as shown in Fig. 10.

5.2. Practical case studies for the proposed charge controller performance validation

To validate the developed solar charge controller for VRFB, the practical solar irradiance profiles have been collected from the solar radiation resource assessment (SRRA) [47] centre installed at the roof top of the IEST, Shibpur campus and applied as input to the controller. The dynamic irradiance data is taken from the Pyranometer installed at the SRRA centre. Irradiance profiles considered in this work are global horizontal irradiance (GHI).

5.2.1. Sunny weather condition

In the first case study, a sunny day is considered and the corresponding dynamic solar insolation profile from 7:00 h to 11:00 h has been monitored as shown in Fig. 11. To avoid over potential and corresponding side reactions inside VRFB stack, the overcharging potential is restricted to 32 V for the 20 Cell 1 kW VRFB system considering 1.6 V/cell. In Fig. 12, the solar PV output power for MPPT charging and the corresponding VRFB charging power are shown. The difference between solar PV power and the VRFB charging power is consumed by the electrical interface system that is the DC-DC buck converter. It is noticed from Fig. 13 that the VRFB state of charge (SOC) is reached up to 75% because of the over potential restriction by the charge controller at 32 V which results in incomplete charging of VRFB. Hence, a throughout charging of VRFB by MPPT topology is not suitable for solar PV power system applications because of battery cycle life degradation due to repetitive incomplete charging.

In Fig. 13, a comparative analysis of VRFB stack terminal voltages for the three different charging topologies has been shown. It may be noted that while charging, the starting SOC is considered at 50% because of the equilibrium potential as shown in Fig. 9. It is found that the VRFB over potential threshold of 32 V is reached at 75% SOC for throughout MPPT charging whereas for the three stage and modified MPPT based three stage CC-CV charging topology, the SOC reaches up to 90% which implies complete charging of VRFB. In the three stage and modified three stage charging, the trickle voltage is set at 29 V and the bulk charging stage is thus applicable up to 32 V. The difference is observed in case of modified three stage charging algorithm and that is in the bulk charging stage where the I_{MPPT} is applied to transfer maximum power from solar PV source to VRFB. In the float charging stage, the voltage across VRFB terminal is kept constant at 32 V till the SOC reaches up to 90%. Corresponding charging current comparison is shown in Fig. 14. Fig. 15a describes the comparison between the charging power transfer capabilities of the three stage (without MPPT in the bulk charging stage) CC-CV and modified three stage (with MPPT in the bulk charging stage) CC-CV charging of VRFB. Fig. 15b shows that the average power transferred from solar PV to VRFB by applying the MPPT enabled three stage CC-CV charge controller is about 55 W more than that of the three stage CC-CV charge controller without MPPT in the bulk charging phase. The charging efficiency is improved from 83% to 94.5% by incorporating the MPPT in the bulk charging stage of the three stage CC-CV charge controller for VRFB. It should be noted that the flow rate is controlled in real time with dynamic charging current to ensure maximum VRFB overall system efficiency and control of stack temperature rise within safe limit.

5.2.2. Cloudy weather condition

In the second case study, the solar PV VRFB charge controller performance is demonstrated under sudden appearance of cloud. As shown in Fig. 16, another practical solar insolation profile on a cloudy day is considered where the cloud appears and sustains within a time frame between 9:00 h and 10:30 h. The performances of the three charge controllers are demonstrated and compared under this dynamic insolation profile. In Fig. 17, the PV output power for MPPT charging and corresponding VRFB charging power are shown. It is further noticed from the Fig. 18 that under cloudy condition the MPPT charge

controller stops charging at the over potential limit of 32 V when the VRFB SOC reaches to near about 73%. This SOC is less than that of MPPT charging in sunny weather condition as shown in the first case study. Hence the problem of incomplete charging is reflected in MPPT charging in this case as well. In Fig. 19, the VRFB stack terminal voltage for all the three charging topologies under cloudy weather condition has been demonstrated. It is observed from Fig. 19 that the VRFB SOC reaches up to 90% for both the three stage and modified three stage charging. Hence the problem of incomplete charging is overcome by applying three stage charging topology. Corresponding charging currents for the three different charging topologies is shown in Fig. 19. Fig. 20a describes the comparison between the charging power transfer capabilities of the three stage CC-CV (without MPPT in the bulk charging stage) and the modified three stage CC-CV (with MPPT in the bulk charging stage) charging of VRFB under sudden appearance of cloud. Fig. 20b shows that the average power transferred from solar PV to VRFB by applying the MPPT enabled three stage CC-CV charge controller is about 45 W more than that of the three stage CC-CV charge controller without MPPT in the bulk charging phase. Thus in this case also, the charging efficiency is improved significantly by incorporating MPPT in the bulk charging stage of the three stage CC-CV charge controller for VRFB. It should be noted that the flow rate is controlled in real time with dynamic charging current as described in section to ensure maximum VRFB overall system efficiency and control of stack temperature rise within safe limit.

6. Conclusion

This paper presents a real time flow control integrated solar PV MPPT based charge controller for Vanadium Redox Flow Battery (VRFB) for the first time and its performance is demonstrated under practical dynamic insolation profiles. The usual Perturb & Observe (P&O) algorithm for designing MPPT charger for conventional batteries like Lead acid, Li-ion etc. has been significantly modified by including the real time control of flow rate for maximizing the VRFB overall system efficiency besides maximizing the charging efficiency. The proposed charging algorithm has been validated by a practical 1 kW 6 h VRFB system and practical. Three different solar PV charging topologies have been implemented for VRFB system and their performances have been compared. It is observed that the modified MPPT based three stage CC-CV charging topology becomes the most efficient for VRFB charging from solar PV source. The charging efficiency is improved from 83% (Conventional three stage CC-CV charging) to 94.5% (Modified three stage CC-CV charging with MPPT in bulk charging phase) by applying suitable MPPT algorithm in the bulk charging stage of VRFB. The complete charging and control of VRFB stack temperature rise within its safe operating limit is also achieved by maintaining the dynamic optimal flow rate. It is observed that by applying constant flow rate during solar PV MPPT charging of VRFB, at an SOC of 74% the VRFB stack temperature rises up to 40 °C where the controller stops working due to thermal shut down for system protection thus leading to incomplete charging. Whereas, by applying dynamic optimal flow rate during MPPT charging, the VRFB stack temperature is maintained within the safe limit of 35 °C and thereby preventing the premature thermal shut down of the controller and incomplete charging. The performance of the controller has been validated by two practical case studies of sunny weather and cloudy weather conditions. The proposed charge controller is a generalised one and thus can be very useful for even large scale VRFB application in solar PV power systems.

Acknowledgement

This research work has been funded by Ministry of New and Renewable Energy (MNRE) Govt. of India and it has been carried out at Centre of Excellence for Green Energy and Sensor Systems, IEST, Shibpur India. The first, second and third author are also thankful to

IEST, India for granting their research fellowship.

References

- [1] Barsali S, Giglioli R, Lutzemberger G, Poli D, Valenti G. Optimised operation of storage systems integrated with MV photovoltaic plants, considering the impact on the battery lifetime. *J Storage Mater* 2017;12:178–85.
- [2] Skyllas-Kazacos M, Kasherman D, Hong D, Kazacos M. Characteristics and performance of 1 kW UNSW vanadium redox battery. *J Power Sources* 1991;35:399–404.
- [3] Cho KT, Tucker MC, Ding M, Ridgway P, Battaglia VS, Srinivasan V, et al. Cyclic performance analysis of hydrogen/bromine flow batteries for grid-scale energy storage. *ChemPlusChem*. 2015;80:402–11.
- [4] De León CP, Frías-Ferrer A, González-García J, Szántó D, Walsh FC. Redox flow cells for energy conversion. *J Power Sources* 2006;160:716–32.
- [5] Leung P, Li X, De León CP, Berlouis L, Low CJ, Walsh FC. Progress in redox flow batteries, remaining challenges and their applications in energy storage. *Rsc Adv* 2012;2:10125–56.
- [6] Arenas L, de León CP, Walsh F. Engineering aspects of the design, construction and performance of modular redox flow batteries for energy storage. *J Storage Mater* 2017;11:119–53.
- [7] Ulaganathan M, Aravindan V, Yan Q, Madhavi S, Skyllas-Kazacos M, Lim TM. Recent advancements in all-vanadium redox flow batteries. *Adv Mater Interfaces* 2016;3.
- [8] Wei L, Zhao T, Zeng L, Zhou X, Zeng Y. Copper nanoparticle-deposited graphite felt electrodes for all vanadium redox flow batteries. *Appl Energy* 2016;180:386–91.
- [9] David O, Percin K, Luo T, Gendel Y, Wessling M. Proton-exchange membranes based on sulfonated poly(ether ether ketone)/polyaniline blends for all-and air-vanadium redox flow battery applications. *J Storage Mater* 2015;1:65–71.
- [10] Reed D, Thomsen E, Wang W, Nie Z, Li B, Wei X, et al. Performance of Nafion® N115, Nafion® NR-212, and Nafion® NR-211 in a 1 kW class all vanadium mixed acid redox flow battery. *J Power Sources* 2015;285:425–30.
- [11] Gattrell M, Park J, MacDougall B, Apte J, McCarthy S, Wu C. Study of the mechanism of the vanadium 4+/5+ redox reaction in acidic solutions. *J Electrochem Soc* 2004;151:A123–30.
- [12] Oriji G, Katayama Y, Miura T. Investigations on V (IV)/V (V) and V (II)/V (III) redox reactions by various electrochemical methods. *J Power Sources* 2005;139:321–4.
- [13] Zhou X, Zhao T, An L, Zeng Y, Yan X. A vanadium redox flow battery model incorporating the effect of ion concentrations on ion mobility. *Applied energy*. 2015;158:157–66.
- [14] Blane C, Rufer A. Understanding the vanadium redox flow batteries. Paths to Sustainable Energy. InTech; 2010.
- [15] Chahwan J, Abbey C, Joos G. VRB modelling for the study of output terminal voltages, internal losses and performance. Electrical Power Conference, 2007 EPC 2007 IEEE Canada. IEEE; 2007. p. 387–92.
- [16] Mohamed M, Ahmad H, Seman MA, Razali S, Najib M. Electrical circuit model of a vanadium redox flow battery using extended Kalman filter. *J Power Sources* 2013;239:284–93.
- [17] Zhang Y, Zhao J, Wang P, Skyllas-Kazacos M, Xiong B, Badrinarayanan R. A comprehensive equivalent circuit model of all-vanadium redox flow battery for power system analysis. *J Power Sources* 2015;290:14–24.
- [18] Bhattacharjee A, Saha H. Design and experimental validation of a generalised electrical equivalent model of Vanadium Redox Flow Battery for interfacing with renewable energy sources. *J Storage Mater* 2017;13:220–32.
- [19] Choudar A, Boukhetala D, Barkat S, Brucker J-M. A local energy management of a hybrid PV-storage based distributed generation for microgrids. *Energy Convers Manage* 2015;90:21–33.
- [20] Bhattacharjee A, Roy A, Banerjee N, Patra S, Saha H. Precision dynamic equivalent circuit model of a Vanadium Redox Flow Battery and determination of circuit parameters for its optimal performance in renewable energy applications [in press]. *J Power Sour* 2018;396C.
- [21] Nguyen TA, Qiu X, Guggenberger II JD, Crow ML, Elmore AC. Performance characterization for photovoltaic-vanadium redox battery microgrid systems. *IEEE Trans Sustain Energy* 2014;5:1379–88.
- [22] Qiu X, Nguyen TA, Guggenberger JD, Crow ML, Elmore AC. A field validated model of a vanadium redox flow battery for microgrids. *IEEE Trans Smart Grid* 2014;5:1592–601.
- [23] Turker B, Klein SA, Hammer E-M, Lenz B, Komsitska L. Modeling a vanadium redox flow battery system for large scale applications. *Energy Convers Manage* 2013;66:26–32.
- [24] Hosseina M, Bathaei SMT. Optimal scheduling for distribution network with redox flow battery storage. *Energy Convers Manage* 2016;121:145–51.
- [25] Turker B, Klein SA, Komsitska L, Trujillo JJ, von Bremen L, Kühn M, et al. Utilizing a vanadium redox flow battery to avoid wind power deviation penalties in an electricity market. *Energy Convers Manage* 2013;76:1150–7.
- [26] Masheleni H, Carelse X. Microcontroller-based charge controller for stand-alone photovoltaic systems. *Sol Energy* 1997;61:225–30.
- [27] Karami N, Moubayed N, Outbib R. Analysis and implementation of an adaptive PV based battery floating charger. *Sol Energy* 2012;86:2383–96.
- [28] Chaieb H, Sakly A. A novel MPPT method for photovoltaic application under partial shaded conditions. *Sol Energy* 2018;159:291–9.
- [29] Kamarzaman NA, Tan CW. A comprehensive review of maximum power point tracking algorithms for photovoltaic systems. *Renew Sustain Energy Rev* 2014;37:585–98.
- [30] Liu Y-H, Chen J-H, Huang J-W. A review of maximum power point tracking techniques for use in partially shaded conditions. *Renew Sustain Energy Rev* 2015;41:436–53.
- [31] Jiang Z, Dougal RA. Multiobjective MPPT/charging controller for standalone PV power systems under different insolation and load conditions. Industry Applications Conference, 2004 39th IAS Annual Meeting Conference Record of the 2004 IEEE. IEEE; 2004. p. 1154–60.
- [32] Mirzaei A, Forooghi M, Ghadimi AA, Abolmasoumi AH, Riahi MR. Design and construction of a charge controller for stand-alone PV/battery hybrid system by using a new control strategy and power management. *Sol Energy* 2017;149:132–44.
- [33] Nafeh AESA. A modified MPPT control loop for PV/battery-charging system using PI controller optimally tuned with GA. *Int J Numer Model Electron Networks Devices Fields* 2011;24:111–22.
- [34] Fathabadi H. Novel high efficiency DC/DC boost converter for using in photovoltaic systems. *Sol Energy* 2016;125:22–31.
- [35] Fathabadi H. Novel photovoltaic based battery charger including novel high efficiency step-up DC/DC converter and novel high accurate fast maximum power point tracking controller. *Energy Convers Manage* 2016;110:200–11.
- [36] López J, Seleme Jr S, Donoso P, Morais L, Cortizo P, Severo M. Digital control strategy for a buck converter operating as a battery charger for stand-alone photovoltaic systems. *Sol Energy* 2016;140:171–87.
- [37] Nguyen T-T, Kim HW, Lee GH, Choi W. Design and implementation of the low cost and fast solar charger with the rooftop PV array of the vehicle. *Sol Energy* 2013;96:83–95.
- [38] Tang A, Ting S, Bao J, Skyllas-Kazacos M. Thermal modelling and simulation of the all-vanadium redox flow battery. *J Power Sources* 2012;203:165–76.
- [39] Yan Y, Li Y, Skyllas-Kazacos M, Bao J. Modelling and simulation of thermal behaviour of vanadium redox flow battery. *J Power Sources* 2016;322:116–28.
- [40] Averbukh M, Pozin A, Sukoriansky S. Electrolyte pumping optimization in already manufactured vanadium redox battery based on experimentally determined electrical and hydrodynamic losses. *J Energy Eng* 2016;143:04016050.
- [41] Li Y, Zhang X, Bao J, Skyllas-Kazacos M. Control of electrolyte flow rate for the vanadium redox flow battery by gain scheduling. *J Storage Mater* 2017;14:125–33.
- [42] Tang A, Bao J, Skyllas-Kazacos M. Studies on pressure losses and flow rate optimization in vanadium redox flow battery. *J Power Sources* 2014;248:154–62.
- [43] You D, Zhang H, Sun C, Ma X. Simulation of the self-discharge process in vanadium redox flow battery. *J Power Sources* 2011;196:1578–85.
- [44] Sun J, Shi D, Zhong H, Li X, Zhang H. Investigations on the self-discharge process in vanadium flow battery. *J Power Sources* 2015;294:562–8.
- [45] Li Y, Zhang X, Bao J, Skyllas-Kazacos M. Studies on optimal charging conditions for vanadium redox flow batteries. *J Storage Mater* 2017;11:191–9.
- [46] Liu K, Li K, Ma H, Zhang J, Peng Q. Multi-objective optimization of charging patterns for lithium-ion battery management. *Energy Convers Manage* 2018;159:151–62.
- [47] <http://www.cwetsolar.com/>.